Smart Structures and Systems, *Vol. 27, No. 3 (2021) 493-506*
DOI: https://doi.org/10.12989/sss.2021.27.3.493

An improved algorithm for pile damage localization based on complex continuous wavelet transform

Jing-Liang Liu [1a], Cheng-Xu Lin [1b], Xi-Jun Ye [2c], Wen-Ting Zheng [3d] and Yong-Peng Luo*[1]

[1] *College of Transportation and Civil Engineering, Fujian Agriculture and Forestry University, Fuzhou 350002, China*
[2] *School of Civil Engineering, Guangzhou University, Guangzhou 510006, China*
[3] *College of Civil Engineering, Fujian University of Technology, Fuzhou 350118, China*

(*Received January 19, 2020, Revised November 11, 2020, Accepted December 9, 2020*)

Abstract. Since the complex continuous wavelet transform (CCWT) based pile damage detection method is empirical and subjective, an improved algorithm for pile damage localization based on CCWT is proposed by introducing K-means clustering and fast Fourier transform (FFT). In this method, the K-means clustering algorithm is used to accurately calculate the time coordinates of two energy concentrating points caused by the incident and reflected waves, respectively. Meanwhile, FFT is employed to estimate the concerned frequency band of the response signal. Therefore, a specific region in the time frequency plane is defined objectively and it can be used to search the phase angle turning points and localize pile damage. The proposed method is verified by numerical examples of piles with single and multiple damage positions. A parameter analysis is also conducted to investigate how damage depth and damage degree in piles affect the accuracy and effectiveness of the proposed method. The results demonstrate that the proposed method is able to localize a pile with a damage at least 2.5 m away from the pile head when the damage degree is as less as 5%. After that, dynamic tests of an actual square reinforced concrete pile and an actual circular reinforced concrete pile are investigated to verify the application of the proposed method on practical engineering. Although the proposed method is capable of localizing actual piles more accurately than the CCWT method, the problem of interference points needs to be addressed by mutual verification with other pile damage localization methods.

Keywords: complex continuous wavelet transform; K-means clustering algorithm; fast Fourier transform; phase angle; damage localization

1. Introduction

As one of the popular types of substructure, pile foundation has been widely applied in high-rise buildings and long-span bridges due to its great bearing capacity. However, practical pile foundations are inevitably affected by working loads and environmental factors during their service life, leading to serious damage even structural failure. If the damage of a pile body cannot be detected in time, more potential catastrophic accidents are likely to happen. Therefore, active measures such as integrity assessment and damage diagnosis are necessary to be taken into account for ensuring the safety of pile foundations (Beskhyroun *et al*. 2010, Seyedpoor *et al*. 2018). Among them, low strain testing is an effective method that has been widely accepted because of its light equipment and high detection efficiency (Massoudi and Teffera 2014, Billet and Sieffert 1989, Poskitt 1991, Olson and Wright 1989). For example, (Kachanov *et al*. 2017) examined the limitations of using sonic echo method for evaluating the integrity of driven concrete piles with near-surface flaws and obtained the criteria for detecting pile flaws in a compact region. (Liu *et al*. 2019a) applied both large-scale indoor model test and discrete element simulation to investigate the dynamic responses of open-ended pipe pile under lateral cyclic loadings and the characteristics of the soil plug and surrounding soil. (Zhang *et al*. 2020) used the low-strain reflected wave method to conduct full-scale model test of X-section cast-in-place concrete pile and analyzed the influence of X-section geometric parameters on three-dimensional velocity responses. In the low strain testing, an impulse load is applied on the top of the pile, resulting in response signals measured by the sensors installed on the pile head. The measured response signals can be interpreted by various signal processing methods, including time domain, frequency domain and etc. Compared with time or frequency domain methods alone, time frequency analysis has an insight into the measured response signals from the prospective of both time and frequency domain. Therefore, it is feasible to introduce some time-frequency signal processing methods for pile integrity assessment and damage detection.

As a new time-frequency signal processing method, wavelet transform has been accepted in the field of pile damage detection (Messina 2008, Beheshti-Aval *et al*. 2011). For example, Park and Kim (2006) improved the

*Corresponding author, Ph.D.,
E-mail: yongpengluo@fafu.edu.cn
[a] Associate Professor, E-mail: liujingliang@fafu.edu.cn
[b] Graduate Student, E-mail: 251026105@qq.com
[c] Ph.D., E-mail: xijun_ye@gzhu.edu.cn
[d] Lecturer, E-mail: mosquito19857@sina.com

ISSN: 1738-1584 (Print), 1738-1991 (Online)

harmonic wavelet analysis method and applied it on nondestructive testing of piles, however, the improved harmonic wavelet analysis method failed in analyzing response signals from piles with minor damage. (Ni *et al*. 2012) used continuous wavelet transform (CWT) to conduct damage identification on piles that have not been buried in soil. Although it achieved good damage localization results, there is still a lack of engineering examples to verify the feasibility of the CWT in detecting minor damages of piles buried in soil. Recently, (Ni *et al*. 2017) proposed a promising method of pile damage identification based on complex continuous wavelet transform (CCWT) and employed it to localize six piles with different damage types. However, the CCWT method is only demonstrated via laboratory tests on pile specimens, and its application on actual piles has not been examined. Moreover, various factors such as pile-soil interaction need to be considered when the CCWT method is applied on actual piles. To address these issues, an experimental verification on an actual pile is investigated by Zheng *et al*. (2020) and a parameter analysis is carried out as well. (Liu *et al*. 2019b) presented a new damage localization method for piles by integrating the analytical mode decomposition (AMD), recursive Hilbert transform (RHT) and complex continuous wavelet transform (CCWT) into a single assessment tool. Compared with the CCWT method, the combined method is capable of localizing pile damage successfully by reducing the effects brought by ambient noise and soil-pile interaction during the low strain test. Typically, the basic principle of the CCWT based pile damage localization method is to extract the information of phase angle turning points from the reflected wave signal, by which the damage position of a pile is successfully detected. However, the CCWT based pile damage localization method has some drawbacks as follows. First, the two energy concentrating points are selected from the wavelet scalogram by a visual inspection and consequently the time coordinates of them are determined subjectively. In addition, the main frequency range of the response signal is also defined by a visualization of wavelet scalogram. Therefore, the CCWT based pile damage localization method can be regarded as an empirical and subjective algorithm. Because of these two problems mentioned above, the specific region used for searching phase angle turning points is not precise, which definitely affects the accuracy of pile damage localization. Second, the CCWT based method was only used for investigating piles with single damage position, however, its application on piles with multiple damage positions has not been illustrated. Moreover, the damage degree and damage depth in piles also have an impact on the accuracy of the CCWT based damage localization method, but how it exactly affects is still in question. Third, few engineering examples can be found to verify the CCWT method, albeit it was demonstrated by numerical examples and laboratory tests of piles. In a word, all the problems mentioned above create challenges for the CCWT based pile damage localization method, thus, it is urgent to solve these problems in terms of the widespread application of this promising method.

To address these issues, an improved algorithm for pile damage localization method based on CCWT is proposed. In this method, the K-means clustering algorithm (Kanungo *et al*. 2002) is first introduced to accurately calculate the time coordinates of the two energy concentrating points from the time-frequency representation, avoiding a subjective selection. In fact, the time coordinates of the two energy concentrating points in the time frequency plane represent the time instances when the incident and reflected wave reach the pile head, respectively. Meanwhile, a fast Fourier transform (Fomchenko *et al*. 2018) (FFT) is also performed on the response signal to obtain a spectrum diagram, by which a frequency band of interest is defined. On a basis of the determination of the time coordinates and the concerned frequency band, a specific area in the time-frequency plane is defined objectively for the searching of phase angle turning points. Second, with a consideration of pile-soil interaction, a numerical example of a concrete pile with single damage position is carried out to illustrate the effectiveness of the proposed method. A simulated concrete pile with two damage positions is also conducted to extend the application of the proposed method in addition to the single damage position case. Moreover, a parameter analysis is performed to investigate how the damage degree and damage depth affect the accuracy of the proposed method. Finally, two dynamic tests of actual piles installed in soil are investigated to verify the application of the proposed method on practical engineering. Compared with the traditional CCWT algorithm, the proposed method has two primary contributions as follows: (1) the determination of the specific area used for searching phase angle turning points is no longer empirical and subjective due to the introduction of the K-means clustering algorithm and FFT; (2) the application of the proposed method is possible to be extended because the dynamic tests of actual piles are performed and the influence factors such as pile-soil interaction, damage position, damage degree and number of damages are investigated as well.

The outline of this paper is as follows. The methodology, including low strain testing, CCWT based pile damage localization method and an improved method for pile damage localization based on CCWT, is presented in Section 2. Numerical examples and dynamic tests of actual piles are investigated to illustrate the proposed method in Section 3 and Section 4, respectively. Conclusions are drawn in Section 5.

2. Methodology

2.1 Low strain testing

In low strain testing, an impulse load (Take *et al*. 1999) is applied on the top of a pile and the resultant response signals are measured by the sensors (Nagayama *et al*. 2007) installed on the pile head. Normally, the measured acceleration response signal is a superposition of is a superposition of the reflected waves from the pile bottom and the damaged position, the incident wave at the pile head and random noises. It can be integrated into a velocity signal, which also provides a great amount of information

for pile damage localization. The impulse load applied on the pile head is usually expressed by a raised cosine impulse function as shown in Eq. (1).

$$P(t)=\begin{cases}\frac{P}{2}\left(1-\cos\frac{2\pi}{T}t\right) & 0\le t\le T\\ 0 & t\le 0 \text{ and } t>T\end{cases} \tag{1}$$

where $P(t)$, t, T and P represent the impulse load, time, pulse width and the amplitude of the impulse load, respectively.

Assuming that the material of the pile is homogeneous and its length-diameter ratio is large enough, the propagation process of the stress wave can be expressed by one-dimensional wave propagation equation (Xu *et al*. 2016) as shown in Eq. (2).

$$\partial^2u(x,t)/\partial x^2-\partial^2u(x,t)/c^2\partial t^2=0 \tag{2}$$

where x represents the coordinate axis of the stress wave propagation direction and $u(x,t)$ denotes the displacement of the particle at the coordinate x and time t. c is the propagation velocity of stress wave with $c^2=E/\rho$, while E and ρ represent the Young's modulus and mass density, respectively (Rausche *et al*. 1991, Niederleithinger and Taffe 2006).

The damage of a pile can be estimated by analyzing the sectional impedance change in a one-dimensional elastic rod, which is expressed as Eq. (3).

$$Z=\rho cA \tag{3}$$

where Z, ρ and A represent impedance, mass density of the pile and area of cross section, respectively.

Typically, any change in E, A, ρ, or a combination of them results in an impedance change or a discontinuity. If the stress wave passes through such a discontinuity, there will be a reflection and transmission at the discontinuous/ damaged cross section. A visualization of the stress wave propagation process can be found in Fig. 1.

As indicated in Fig. (1), the transmitted formula of the stress wave can be expressed as Eqs. (4) and (5) on an assumption that the impedance changes from Z_1 (intact section) to Z_2 (damaged section).

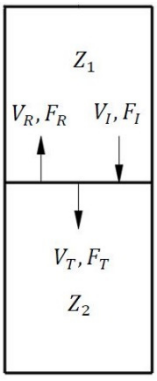

Fig. 1 The reflection and transmission of the stress wave at the damaged section

$$V_I+V_R=V_T \tag{4}$$

$$F_I+F_R=F_T \tag{5}$$

where V and F represent the vibration velocity and force at the interface of the particle, respectively. The subscripts of I, R and T separately denote the incident wave, reflected wave and transmitted wave. According to the momentum conservation law of wavefront, $F_I=-Z_1V_I$, $F_R=Z_1V_R$ and $F_T=-Z_2V_T$ are obtained and they can be substituted into Eqs. (4) and (5) to get Eqs. (6) and (7), respectively (Xu *et al*. 2016).

$$Z_1V_I-Z_1V_R=Z_2V_T \tag{6}$$

$$F_I/Z_1-F_R/Z_1=F_T/Z_2 \tag{7}$$

By establishing a simultaneous equation composed of Eqs. (4)~(7), the vibration velocity of the reflected wave (V_R) and the sectional force of the reflected wave (F_R) are solved and expressed as Eqs. (8) and (9) (Xu *et al*. 2016).

$$F_R=F_I\,(Z_2-Z_1)/(Z_1+Z_2) \tag{8}$$

$$V_R=V_I\,(Z_1-Z_2)/(Z_1+Z_2) \tag{9}$$

2.2 CCWT based pile damage localization method

Compared with the amplitude information, the phase information of the reflected wave is more sensitive to damage (Ni *et al*. 2017). The wavelet transform enable the phase extraction because it not only inherits the ideas of Gabor transform partially but also provides a flexible time-frequency window. Moreover, the complex Gaussian wavelet transform is especially suitable for analyzing the phase information of response signals due to its complex wavelet basis function (Ni *et al*. 2017). The mathematical expression of the complex Gaussian wavelet function is expressed in Eq. (10).

$$\psi(t)=C_pe^{t^2}e^{-\mathrm{j}t} \tag{10}$$

where C_p is the scaling parameter when $|\psi(t)^{(p)}|^2=1$ and $\psi(t)^{(p)}$ represents the p-th derivative of $\psi(t)$.

If $\psi(t)$ is a given square-integrable parent complex wavelet function and satisfies the admissibility condition, the CCWT of an arbitrary response signal $x(t)$ can be defined as

$$W_x(a,b)=\int_{-\infty}^{+\infty}x(t)\frac{1}{\sqrt{a}}\overline{\psi(\frac{t-b}{a})}\mathrm{d}t \tag{11}$$

where a and b are the scale factor and the dilation factor, respectively, and $\overline{\psi\left(\frac{t-b}{a}\right)}$ represents the complex conjugate of $\psi\left(\frac{t-b}{a}\right)$.

According to Eq. (11) the instantaneous phase angle $\phi(t)$ of $W_x(a,b)$ is calculated as

$$\phi(t)=\arctan\left[\frac{W_I(a,b)}{W_R(a,b)}\right] \tag{12}$$

where $W_I(a,b)$ and $W_R(a,b)$ represent the imaginary part and the real part of $W_x(a,b)$, respectively.

Based on Eq. (12), the phase angles of the wavelet coefficients are obtained and then mapped into the time-frequency plane to get the grayscale images of phase angles, in which white color denotes 180 degree (π) of phase angle and black color indicates -180 degree ($-\pi$) of phase angle (Boulahbal *et al*. 1999). In the grayscale image, the phase angle curve exhibits a set of equidistant lines when the material of the pile body is uniform and undamaged. By contrast, there will be an appearance of "crossing points" if the pile is damaged (Boulahbal *et al*. 1999). To further verify these crossing points, the time-phase angle curve at a specific frequency is calculated. In fact, the phase angle turning point in the time-phase angle curve could be regarded as the real damage point only when the energy related to the crossing point exists. After that, the time difference between the phase angle turning point and the energy concentrating point caused by the incident wave, denoted as Δt_n, is calculated. With the solution of Δt_n, L_n can be computed according to the one-dimensional wave theory and thus expressed as Eq. (13) (Ni *et al*. 2017).

$$L_n = \frac{1}{2} \times c \times \Delta t_n \tag{13}$$

where L_n represents the distance between the damaged position and the pile head.

2.3 An improved method for pile damage localization based on CCWT

In Section 2.2, the time difference between the phase angle turning point and the top of the pile is determined subjectively due to that the time instances of both the phase angle turning point and the energy concentrating point are defined by visually inspecting the phase angle curve and the wavelet scalogram, respectively. Hence, the CCWT based pile damage localization method cannot be regarded as an objective and accurate approach, which really affects its application on the damage localization of actual piles. In fact, the energy concentrating regions caused by the incident and reflected waves are not two single point but large areas with bright colors, therefore, it is not appropriate to determine the optimum energy concentrating points only by visualization. In addition, the response signal is not a narrow-band but a wide-band signal, which creates challenges for the definition of the concerned frequency band by visually inspecting the scalogram alone. In order to address these issues, an improved algorithm for pile damage localization based on CCWT is proposed and its flowchart is presented in Fig. 2.

At first, the wavelet coefficients are extracted by performing CCWT and then mapped into the wavelet scalogram. The color in the wavelet scalogram represents the magnitude of the modulus or energy. That is to say, the bright color indicates higher energy, while the dark color denotes lower energy. In the wavelet scalogram, there are two bright energy concentrating areas that are caused by the incident wave at the pile head and the reflected wave at the bottom of the pile, respectively. Therefore, clustering methods instead of visual inspections are employed to accurately determine the central point of the energy concentrating area. As a typical distance-based clustering algorithm, K-means clustering algorithm is capable of clustering the bright energy concentrating areas which is represented by the modulus values of wavelet coefficients. Since there are two bright energy concentrating areas in the wavelet scalogram, the clusters can be divided into two categories and the number of clusters K is set to be 2. At the beginning, two points are randomly selected as the initial clustering centers. The distances between the remaining points and the two clustering centers are then calculated and each remaining point is assigned to the nearest clustering center according to the calculated distances (Please see Eq. (14)). With this, all points are divided into two clusters and the mean value of the points in each cluster is computed and defined as the new clustering center. If the distance between the new and old clustering center is longer than the preset threshold (usually recommended as 1×10^{-7}), the new clustering center will be defined as the initial clustering center once again and the clustering process is repeated in the next step. Otherwise, the clustering process is finished and the two clustering center is finally determined. As such, the two new clustering centers determined in the final step can be regarded as the two energy concentrating points and their corresponding time coordinates are denoted as the time instances when the incident and the reflected wave reach the pile head, respectively.

$$f(x_i) = \arg\min \sum_{j=1}^{k} \sum_{x_i \in C_j} \left\| x_i - u_j \right\|^2 \tag{14}$$

where u_j and x_i represent the initial clustering centers and the remaining points, respectively. $f(x_i)$ denotes the minimum sum of squared distances.

Meanwhile, the response signal is processed by FFT, resulting in many peak points in the Fourier spectrum. However, the frequency range we are concerned is narrow but not wide when compared with the whole frequency axis. Thus, the frequency band of interest is determined by the first and last peak points in the Fourier spectrum, leading to that the frequencies out of the range of interest are ignored. In fact, the frequency beyond the range of interest is usually caused by the noises and other factors hidden in the response signal, therefore, an ignorance of the influence from the noises and a restriction of the frequency band are thought to be reasonable.

With the introduction of the K-means clustering algorithm and FFT, the specific region is determined from both time and frequency direction, thus, the damage localization process can be performed in a similar way to that of Section 2.2. By finding the phase angle turning point in the time-phase angle curve, the time difference $\Delta t_n'$ between the phase angle turning point and the energy concentrating point caused by the incident wave is calculated. After that, the distance (L_n') between the damaged section and the pile head can be computed by using $\Delta t_n'$ instead of Δt_n (Ni *et al*. 2017).

$$L_n' = \frac{1}{2} \times c \times \Delta t_n' \tag{15}$$

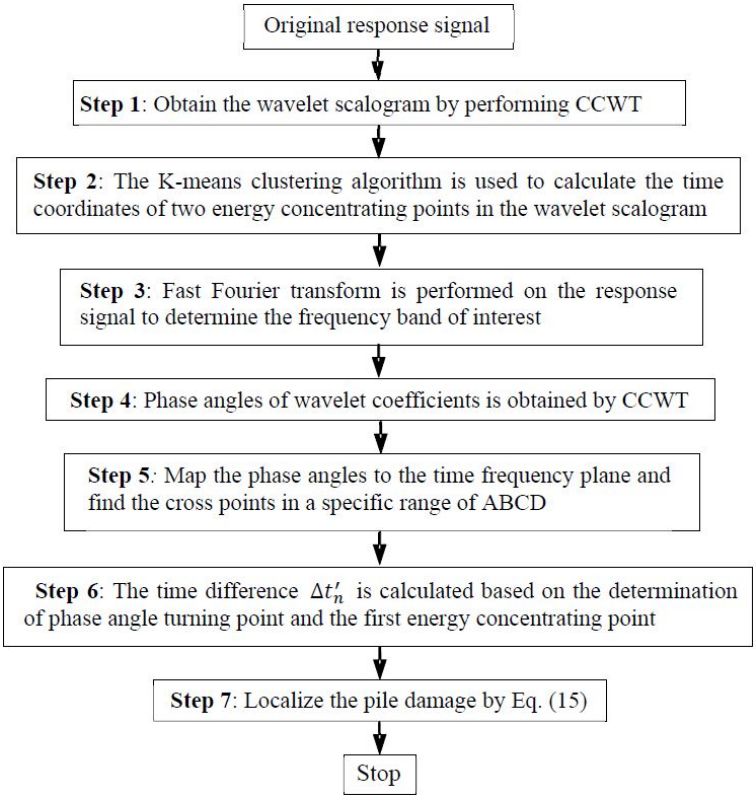

Fig. 2 The flowchart of the improved method for pile damage localization based on CCWT

3. Numerical examples

3.1 The concrete pile model considering pile-soil interaction

In order to indicate how to establish a 3D finite element (FE) model of piles with a consideration of pile-soil interaction, an intact concrete pile as shown in Fig. 3 is simulated by ABAQUS at first (Kim *et al*. 2012). The materials of the pile body and the soil are separately concrete and clay, whose properties are shown in Table 1 (Wolf and Arx 1982). The length of the pile is set as 20 m and the diameter is 1 m, of which 18 m is buried in the soil. To consider the pile-soil interaction and obtain more realistic response signals, face-to-face contact is adopted between the pile and soil in this model. Actually, two contact behaviors, including tangential behavior and normal behavior, are considered. The friction coefficient of the tangential behavior is set as 0.4, and the normal behavior is set as hard contact. Since the length-diameter ratio of the pile model with homogeneous material (concrete) is large enough, the low strain testing based on one-dimensional wave propagation theory is appropriate to be used for pile integrity assessment. The diameter of the surrounding soil is 5 times that of the pile, which is large enough to avoid the influence of waves that reflected from the far-field boundary back to the sensor (Cabella and Passalacqua 1998).

Before the dynamic analysis, the horizontal displacement of the soil located at the outer surface is restrained and the bottom surface of the soil is completely consolidated. By contrast, the horizontal displacement of the pile body's outer surface is restrained and the vertical displacement of the whole pile body is retained. After that, the gravity load is applied to the pile-soil model, while the raised cosine impulse function is used as the initial excitation on the pile head.

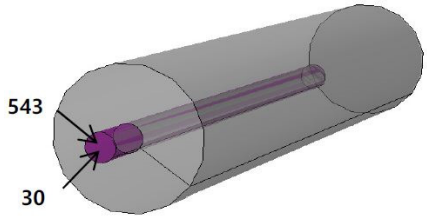

Fig. 3 The FE model of the intact pile (the purple and grey indicate the pile and soil, respectively)

Table 1 The material properties of the concrete pile and soil

Properties	Concrete pile	Soil
Young's modulus	4×10^4 MPa	18 MPa
Poisson's ratio	0.2	0.38
Density	2500 kg/m^3	1800 kg/m^3
Friction angle	/	24°
Cohesion yield stress	/	72 kPa

3.2 Single damage position

In this case, only FE model of a pile with single damage position as shown in Fig. 4 is developed. The definition of

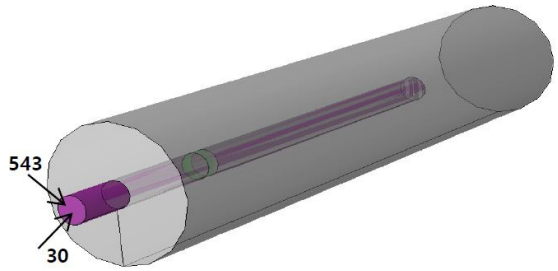

Fig. 4 The FE model of the pile with single damage (the purple, grey and green indicate the pile, soil and damaged section, respectively)

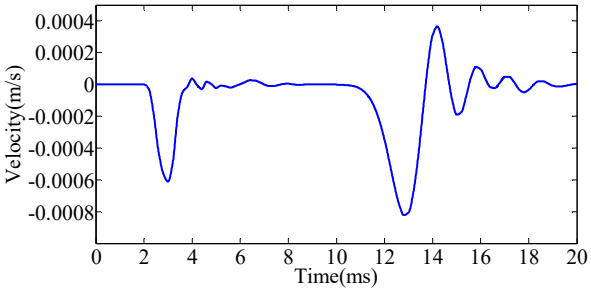

Fig. 5 The velocity response signal

properties, contacts, constraints and loads is identical to that of the intact concrete pile model, however, the damage type of the pile body is defined as necking, with the diameter of the necking section set as 0.95 m. That is to say, the damage degree of this section is around 10%. The damage depth is 0.5 m and located at 6~6.5 m from the top of the pile. The impulse load is applied on the center of the pile head (Node 30 in Fig. 4) at 2 ms, with its amplitude and width are 5 kN and 1.6 ms, respectively. The time interval is set to be 0.2 ms and the total duration of time is defined as 20 ms. After that, the velocity response signal at Node 543 (near the center point) is computed by implicit dynamic analysis and plotted in Fig. 5. It should be noted here that similar results can be obtained whatever the displacement or acceleration response signal is employed. For simplicity, only the velocity response signal is used in the numerical example.

After the velocity response signal at Node 543 is selected as the target signal, the CCWT is performed on it with complex Gaussian wavelet as parent wavelet function. The resultant wavelet scalogram is presented in Fig. 6. It can be seen from Fig. 6 that there are two distinct bright color energy concentrating areas in the time frequency plane. The brighter the color, the larger the modulus of the wavelet coefficients (energy). To be honest, it is really hard to select the time coordinates of the two bright energy concentrating regions by direct visualization. Thus, the K-means clustering algorithm is introduced to address this issue. First of all, the wavelet scalogram is cut into two parts vertically by a straight line which is parallel to the frequency axis and located at an arbitrary position between the two concentrating areas, e.g., t = 6 ms (red line in Fig. 6). The left part is the first energy concentrating area caused by the incident wave, while the right part is the second energy concentrating area trigged by the reflected wave. As

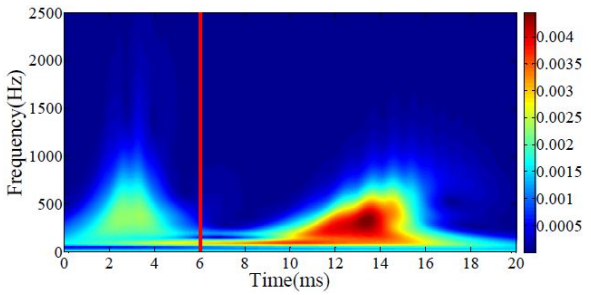

Fig. 6 The wavelet scalogram of the velocity response signal

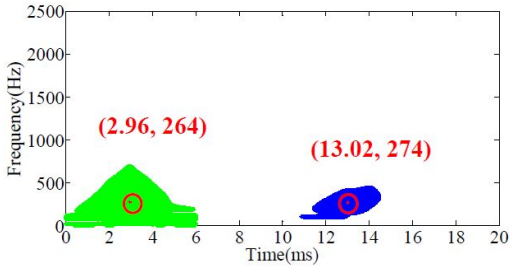

Fig. 7 The results after the K-means clustering

indicated in Fig. 6, different colors in the color bar represent different values, which can be used as thresholds to define the clustering ranges. Here, the critical threshold of the wavelet coefficient modulus in the left part is set to be 0.0015, while that of the right part is defined as 0.003. Actually, the selection of the critical thresholds does not have a great impact on the clustering results, which is further investigated at the end of this section and shown in Table 2. Then, the wavelet coefficients in the two divided energy concentrating regions are extracted and clustered by the K-means clustering algorithm if their modulus is larger than the preset threshold. The results after the K-means clustering are plotted in Fig. 7. As shown in Fig. 7, the time coordinates of the two clustering centers in the time-frequency plane are 2.96 ms and 13.02 ms, respectively. The clustering center at 2.96 ms is caused by the incident wave, while the clustering center at 13.02 ms is triggered by

Table 2 The results under different clustering ranges

Clustering range	Critical threshold of the first part	Critical threshold of the second part	Time coordinates of two energy concentrating centers
C1	0.0015	0.0020	2.96 ms and 13.49 ms
C2	0.0015	0.0025	2.96 ms and 13.17 ms
C3	0.0015	0.0030	2.96 ms and 12.99 ms
C4	0.0015	0.0035	2.96 ms and 13.02 ms
C5	0.0015	0.0040	2.96 ms and 12.86 ms
C6	0.0020	0.0020	3.25 ms and 13.49 ms
C7	0.0020	0.0025	3.25 ms and 13.17 ms
C8	0.0020	0.0030	3.25 ms and 12.99 ms
C9	0.0020	0.0035	3.25 ms and 13.02 ms
C10	0.0020	0.0040	3.25 ms and 12.86 ms

the reflected wave at the bottom of the pile. Meanwhile, the target signal is processed by FFT, leading to a Fourier spectrum as shown in Fig. 8. According to the first and last peak points displayed in the Fourier spectrum, the frequency band of interest can be determined as 100 Hz~750 Hz. So far, the searching range of the crossing points is objectively restricted to the area of 2.96 ms~13.02 ms and 100 Hz~750 Hz in the time-frequency plane, which has a name of ABCD and is shown in Fig. 9.

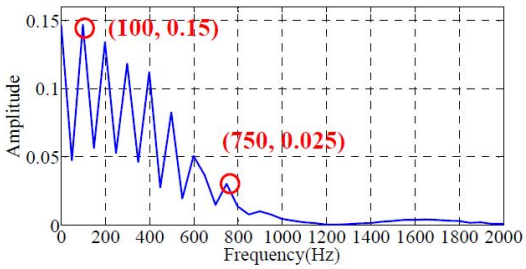

Fig. 8 The Fourier spectrum

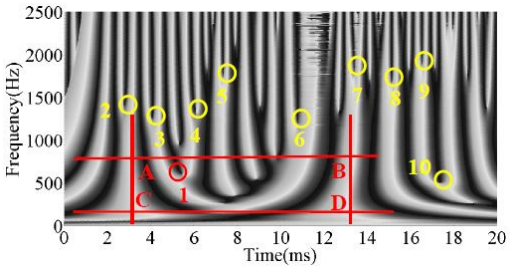

Fig. 9 The grayscale images of phase angles

The wavelet coefficients are also used to calculate instantaneous phase angles based on Eq. (12) after the CCWT is performed on the target signal. The calculated instantaneous phase angles are then mapped into the time-frequency plane and displayed in Fig. 9 in the manner of gray level. We search the crossing points in the range of ABCD (please see Fig. 9), and hence obtain one crossing point (Point 1) whose frequency coordinate falls in the range from 550 Hz to 600 Hz. Theoretically, a crossing point can be recognized as a phase angle turning point only when the energy related to the crossing point exists. Otherwise, this crossing point is regarded as a fake point. To further verify these crossing points, the time-phase angle curves at 550 Hz~600 Hz are calculated and the results are plotted in Fig. 10. It can be seen from Fig. 10 that the time coordinates of all phase angle turning points at 550, 560, 570, 580, 590, 600 Hz are nearly the same, but the degree of the phase turning at 600 Hz is the largest. Consequently, the time-phase angle curve at Fig. 10(e) (600 Hz) is used to localize pile damage. As can be seen from Fig. 10(e), the

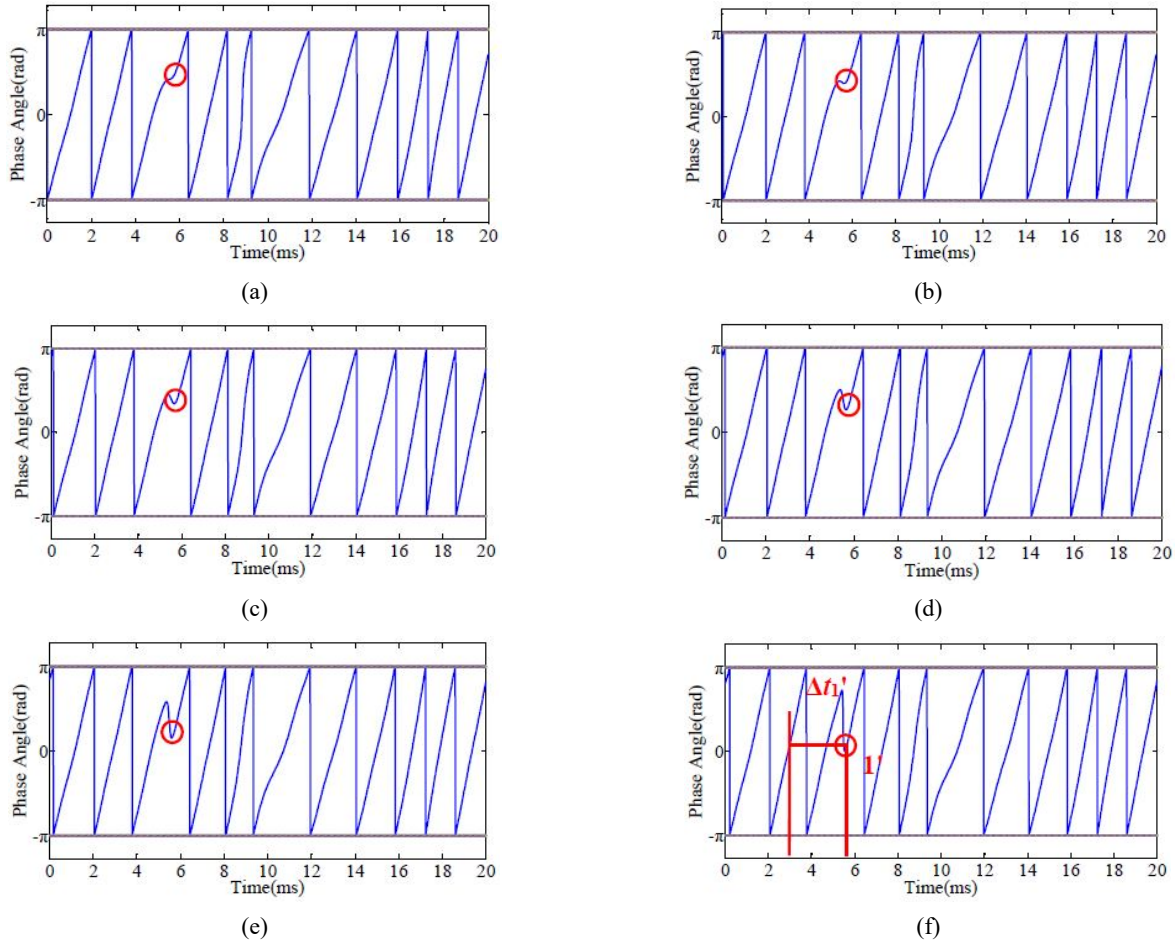

Fig. 10 The time-phase angle curve at the frequencies: (a) 550 Hz; (b) 560 Hz; (c) 570 Hz; (d) 580 Hz; (e) 590 Hz; (f) 600 Hz

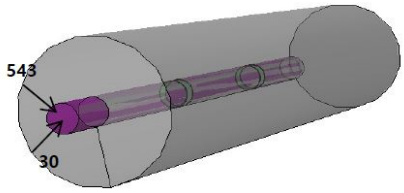

Fig. 11 The FE model of the concrete pile with multiple damage positions (the purple, grey and green indicate the pile, soil and damaged position, respectively)

phase angle turning point corresponding to Point 1 is Point 1' with a time instance of 5.65ms. Therefore, the time duration between the phase angle turning point (Point 1') and the first clustering center induced by the incident wave, denoted as $\Delta t_1'$, is 2.69 ms (5.65 – 2.96 = 2.69 ms). Since the stress wave propagation velocity c equals 4000 m/s by using $c = \sqrt{E/\rho}$, the distance from the damaged position to the top of the pile (L_1') is solved to be 5.38 m by substituting $\Delta t_1'$ and c into Eq. (15). That is to say, the damage is possible to appear at 5.38 m away from the pile head, which is in good accordance with the preset damage position (6 m away from the pile head) and the relative error is only 10.33%.

Besides Point 1, there are other nine crossing points named as Point 2~10 in Fig. 9, however, they all fall outside the range of ABCD. Therefore, a conclusion can be drawn that the proposed method is capable of reducing even eliminating the interference points by a precise definition of the specific region (ABCD) when compared with the CCWT method. Moreover, the definition of the specific area is no longer empirical but objective, which in turn enhances the accuracy of pile damage localization.

It should be noted that different colors in the color bar of Fig. 6 represent various values. Thus, different clustering ranges can be investigated by selecting various critical thresholds according to the values displayed in the color bar. In order to verify the robustness of the K-means clustering algorithm, 10 initial clustering ranges, expressed as C1~C10, are designed and detailed in Table 2. It is shown in Table 2 that the time coordinates of the clustering centers obtained by the K-means clustering algorithm are very close regardless of the initial clustering range. That is to say, the initial clustering range has few impacts on the final pile damage localization results, which definitely demonstrates the robustness of the K-means clustering algorithm.

3.3 Multiple damage positions

A simulated concrete pile with two damage positions is considered in this section and its 3D FE model is presented in Fig. 11. The definition of properties, contacts, constraints, loads and damage types is the same as that in Section 3.2. The only difference is that the distances from the two simulated damage positions to the pile head are 8m and 15 m, respectively. The velocity response signal of the reflected wave near the center of the pile head (Node 543) as shown in Fig. 12 is obtained by implicit dynamic

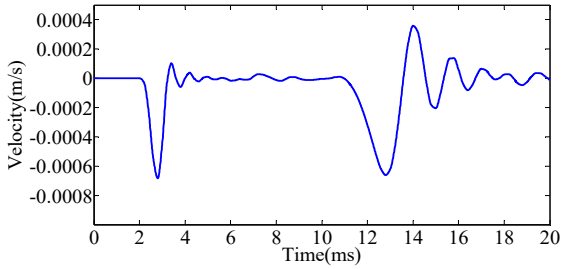

Fig. 12 The velocity response signal

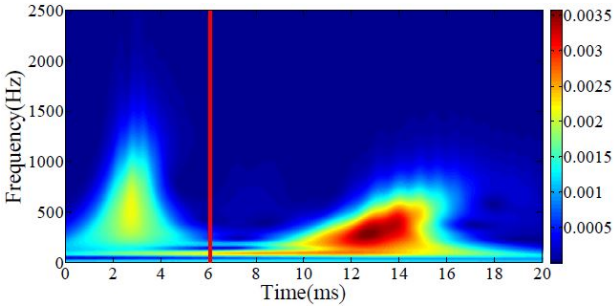

Fig. 13 The wavelet scalogram of the velocity response signal

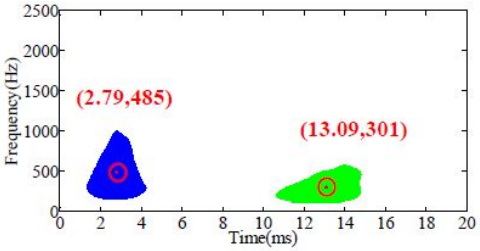

Fig. 14 The results after the K-means clustering

analysis.

The complex Gaussian continuous wavelet transform is first performed on the velocity response signal in Fig. 12 and the resultant wavelet scalogram is plotted in Fig. 13. It can be seen from Fig. 13 that there are two bright energy concentrating areas in the wavelet scalogram. Then, the scalogram is divided into two parts vertically by a straight line of t = 6 ms (red line in Fig. 13). Although various values can be selected as critical thresholds to predefine the clustering range due to the robustness demonstrated before, the critical threshold of the wavelet coefficient modulus in the first energy concentrating region is set to be 0.0015, while that of the second concentrating region is predefined as 0.0025. After that, the wavelet coefficient modulus larger than the preset threshold is extracted and clustered by the K-means clustering algorithm, and the resultant data points are shown in Fig. 14. As shown in Fig. 14, the time coordinates of the two clustering centers in the time-frequency plane are 2.79 ms and 13.09 ms, respectively. The clustering center at 2.79 ms is caused by the incident wave, while the counterpart caused by the reflected wave at the pile bottom is 13.09 ms. In the meantime, the velocity response signal in Fig. 12 is processed by FFT to obtain the Fourier spectrum as shown in Fig. 15. According to the first

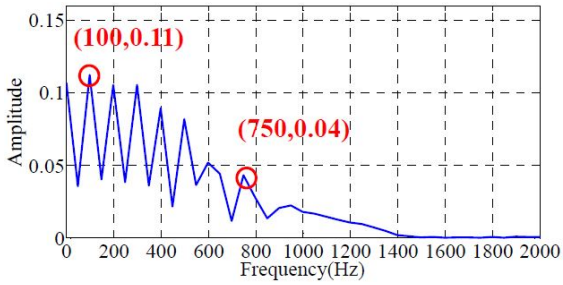

Fig. 15 The Fourier spectrum

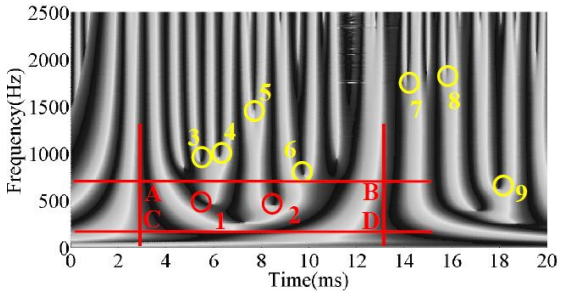

Fig. 16 The grayscale images of phase angles

and last two peak points in the Fourier spectrum, the frequency band of interest can be determined as a range from 100 Hz to 750 Hz. As such, the searching range of the crossing points in the time-frequency plane is 2.79 ms~13.09 ms and 100 Hz~750 Hz, which we define as ABCD in Fig. 16.

Because of the complex Gaussian continuous wavelet transform performed before, the resultant phase angles can be calculated based on Eq. (12). Then, they are mapped into the time-frequency plane and displayed in Fig. 16 in the manner of gray level. We search crossing points in the range of ABCD and get Points 1 and 2, whose frequency coordinates both correspond to 420 Hz~440 Hz. To further validate these two crossing points, the time-phase angle curve at a specific frequency of 440 Hz is calculated and displayed in Fig 17. It is shown in Fig. 17 that the phase angle turning points corresponding to Points 1 and 2 are Points 1' and 2', respectively. The time coordinates of the two phase angle turning points (Points 1' and 2') are 6.1 ms and 9 ms, respectively. Therefore, the time duration between Point 1' and the first clustering center induced by the incident wave, denoted as $\Delta t_1'$, is 3.31 ms (6.1 – 2.79 = 3.31 ms). Similarly, the time duration between Point 2' and the first clustering center, denoted as $\Delta t_2'$, is 6.21 ms (9-2.79 = 6.21 ms). Since the stress wave propagation velocity c equals 4000 m/s by using $c = \sqrt{E/\rho}$, the distance from the damaged position to the top of the pile (L_1') is then calculated to be 6.62 m by substituting $\Delta t_1'$ and c into Eq. (15). L_2' can be solved in a similar way and equals 12.42 m. The damage localization results basically agree with the preset damage positions (8 m and 15 m away from the pile head) and the relative errors are 17.25% and 17.2%, respectively. Compared with the case of single damage position, the proposed method is also capable of localizing piles with two damage positions, however, its accuracy has

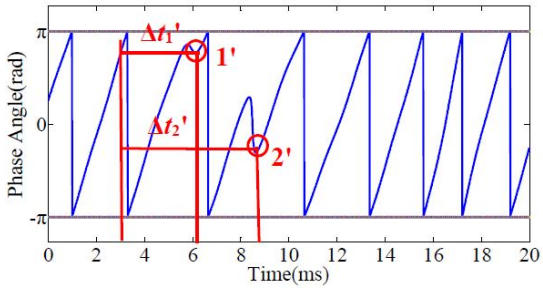

Fig. 17 The time-phase angle curve at the frequency of 440 Hz

a decrease.

In addition to Points 1 and 2, there are other seven crossing points falling outside the range of ABCD. These extra crossing points are named as Points 3~9 in the grayscale image (Fig. 16) and cannot be reduced or eliminated by the traditional CCWT method. Due to the fact that the specific area is no longer defined empirically but objectively, the crossing points are reduced and the accuracy of the pile damage localization is greatly improved.

3.4 Parameter analysis

In Section 3.2 and 3.3, only a pile with single damage position at 6 m from the top of the pile and a pile with multiple damage positions at 8 m and 15 m from the pile head are considered. In order to verify the effectiveness and accuracy of the proposed method under different damage depths and damage degrees, 18 damage scenarios named as DS1~DS18 are designed and detailed in Table 3. Based on the theory that narrower impulse loads are conducive in detecting shallow damages of piles and wider impulse loads are helpful on the localization of deep damages in piles, different impulse widths are considered according to different damage depths. Then, the proposed method is used to analyze the response signals under different damage scenarios, leading to the damage localization results as shown in Table 3.

It can be seen from Table 3 that the proposed method is capable of localizing the pile body when the damage degree is 10%. By contrast, most damages are detected successfully if the damage degree is 5%, however, the relative error of the damage localization result in DS10 is too large (74%) to be accepted by practical engineering. The reason for this phenomenon is that the damage position in DS10 is too close (2 m) to the pile head. When the damage position is too close to the pile head, the excessive energy of the incident wave generated by the hammer is possible to conceal the phase information (e.g., phase turning points) near the pile head, which will bring some errors to the pile damage detection results. Therefore, a conclusion can be drawn that the proposed method is capable of localizing the pile with damage degree as less as 5% on a premise that the damage is at least 2.5 m away from the top of the pile (0.5 m away from the soil surface). It should be noted here that this conclusion only acts in this numerical example and its effectiveness needs more validation in ways of both simulations and dynamic tests.

Table 3 Damage localization results under different damage scenarios

Damage scenarios	Damage type	Damage depth	Damage degree	Amplitude of load	Pulse width	Effectiveness	Relative error
DS1		2.0 m			0.3 ms	Yes	24.00%
DS2		2.5 m			0.4 ms	Yes	19.20%
DS3		3.0 m			0.4 ms	Yes	18.00%
DS4		3.5 m			0.8 ms	Yes	15.43%
DS5	Necking	4.0 m	10%	5kN	0.8 ms	Yes	15.00%
DS6		4.5 m			1.2 ms	Yes	14.67%
DS7		5.0 m			1.2 ms	Yes	14.00%
DS8		5.5 m			1.6 ms	Yes	13.45%
DS9		6.0 m			1.6 ms	Yes	10.33%
DS10		2.0 m			0.3 ms	No	74.00%
DS11		2.5 m			0.4 ms	Yes	36.80%
DS12		3.0 m			0.4 ms	Yes	33.30%
DS13		3.5 m			0.8 ms	Yes	21.10%
DS14	Necking	4.0 m	5%	5kN	0.8 ms	Yes	20.00%
DS15		4.5 m			1.2 ms	Yes	15.56%
DS16		5.0 m			1.2 ms	Yes	15.20%
DS17		5.5 m			1.6 ms	Yes	14.55%
DS18		6.0 m			1.6 ms	Yes	13.33%

It can be seen from Table 3 that the proposed method is capable of localizing the pile body when the damage degree is 10%. By contrast, most damages are detected successfully if the damage degree is 5%, however, the relative error of the damage localization result in DS10 is too large (74%) to be accepted by practical engineering. The reason for this phenomenon is that the damage position in DS10 is too close (2 m) to the pile head. Thus, a conclusion can be drawn that the proposed method is capable of localizing the pile with damage degree as less as 5% on a premise that the damage is at least 2.5 m away from the top of the pile (0.5 m away from the soil surface). It should be noted here that this conclusion only acts in this numerical example and its effectiveness needs more validation in ways of both simulations and dynamic tests.

4. Dynamic tests

4.1 Damage localization of an actual square reinforced concrete pile

A low strain test of an actual pile in the pile testing base of Fujian University of Technology is performed in this section to verify the effectiveness of the proposed method. The pile to be analyzed is a square reinforced concrete pile with a lateral length of 0.2 m. The length of the pile is 8 m and it is wholly buried into soil horizontally. Before embedding the pile into the soil, the pile was necked at 4~4.2 m away from the pile head and it can be taken as the theoretical result for comparison. Since the length-diameter ratio of the pile is large enough, the premise of one-dimensional wave theory is satisfied. The response of the

Fig. 18 The setup of the pile test

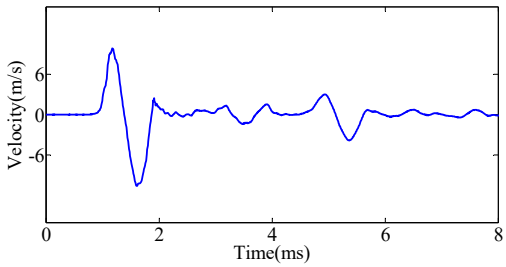

Fig. 19 The velocity response signal

stress wave is excited by a hammer and measured by an ICP accelerometer with a sensitivity of 19.6 mV/m/s^2, which is installed on the pile head and shown in Fig. 18. The wave propagation velocity c is solved as 3800 m/s based on the properties of the reinforced concrete pile. The data acquisition system used here is the ZBL-P8100 pile integrity tester manufactured by the Beijing Zhibolian Company in China. In this test, the acceleration response

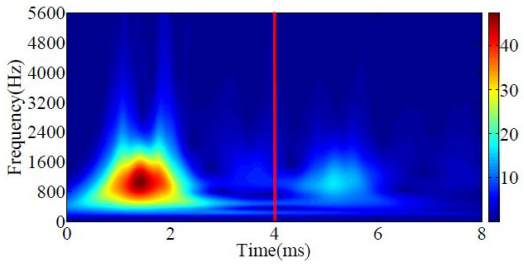

Fig. 20 The wavelet scalogram of the velocity response signal

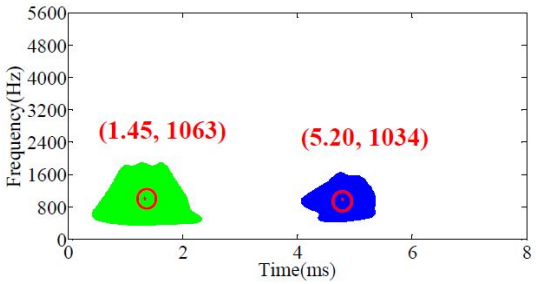

Fig. 21 The results after the K-means clustering

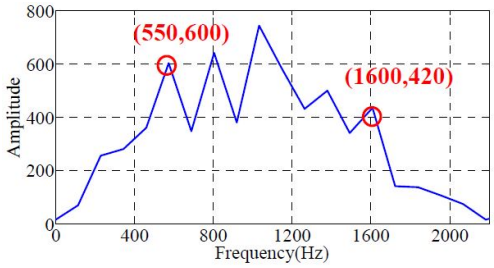

Fig. 22 The Fourier spectrum

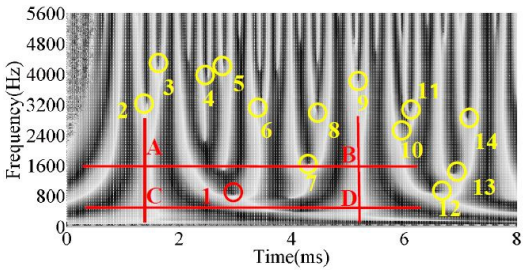

Fig. 23 The grayscale images of phase angles

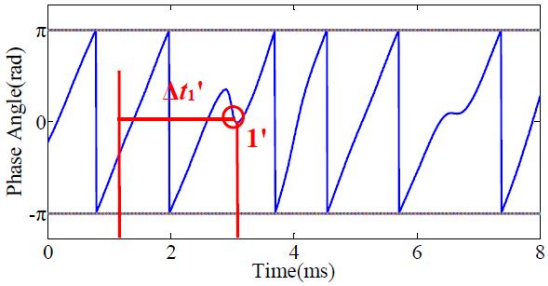

Fig. 24 The time-phase angle curve at the frequency of 804 Hz

was measured with a time interval of 8.5 μs, that is, the sampling frequency is around 118 kHz. Base on the collected acceleration data, the velocity signal as shown in Fig. 19 can be obtained by integration.

The complex Gaussian continuous wavelet transform is first performed on the velocity response signal in Fig. 19 and the resultant wavelet scalogram is plotted in Fig. 20. It can be seen from Fig. 20 that there are two energy concentrating areas with bright colors in the time frequency plane. The scalogram is cut into two parts vertically by a straight red line (t = 4 ms). By setting the critical thresholds of the modulus of the wavelet coefficients in the first and second energy concentrating regions as 17 and 30, respectively, the modulus of the wavelet coefficients larger than the preset thresholds are extracted and clustered by the K-means clustering algorithm, resulting in the clustering data points as shown in Fig. 21. As indicated in Fig. 21, the time coordinates of the two clustering centers in the time-frequency plane are 1.45 ms and 5.20 ms, respectively. The clustering center at 1.45 ms is caused by the incident wave, while the clustering center at 5.20 ms is caused by the reflected wave at the bottom of the pile. Meanwhile, the velocity response signal is processed by FFT to obtain the Fourier spectrum as shown in Fig. 22. According to the frequency coordinates corresponding to the first and last two peak points in the Fourier spectrum, the concerned frequency band is defined as 550 Hz~1600 Hz. Thus, the searching range of the phase angle turning points is 1.45 ms~5.20 ms and 550 Hz~1600 Hz, which is denoted as ABCD and shown in Fig. 23.

After the complex Gaussian continuous wavelet transform is performed on the velocity response signal in Fig. 19, the phase angle can be calculated according to Eq. (12). The resultant instantaneous phase angles are then mapped into the time-frequency plane and displayed in Fig. 23 in the manner of gray level. By searching the "crossing points" from the range of ABCD in Fig. 23, one crossing point is found and named as Point 1, with its frequency coordinate corresponding to 747 Hz~804 Hz. After that, the phase angle curve at a specific frequency (804 Hz) is calculated and displayed in Fig. 24. It is shown in Fig. 24 that the phase angle turning point corresponding to Point 1 is Point 1', and its time coordinate is 3.1 ms. Therefore, the time duration between the phase angle turning Point 1' and the pile head, denoted as $\Delta t_1'$, is 1.65 ms (3.1 – 1.45 = 1.65 ms). After the wave propagation velocity c is calculated as 3800 m/s with a use of the properties of the reinforced concrete pile, L_1' equals 3.14 m by substituting $\Delta t_1'$ and c into Eq. (15). That is to say, the damage is possible to appear at 3.14 m away from the pile head. The damage localization result is basically consistent with the preset damage position (4 m away from the pile head), with a relative error of 21.5%.

There are other thirteen crossing points in the grayscale image in addition to Point 1, which we named as Points 2~14 in Fig. 23. However, they all fall outside the range of ABCD, which reinforces the fact that the proposed method is capable of reducing extra crossing points caused by other factors while the CCWT does not work on it. Because of the

introduction of K-means clustering method and FFT, the specific region (ABCD) is defined precisely and objectively, leading to a better pile damage localization result than the CCWT method.

4.2 Damage localization of an actual circular reinforced concrete pile

In this section, a low strain test of an actual pile located at the Metro Line 6 of Fuzhou City, Fujian Province of China is performed. The pile to be analyzed is a circular reinforced concrete pile with a diameter of 1 m and a length of 22 m. Therefore, the length-diameter ratio of pile equals 22, which satisfies the premise of one-dimensional wave theory. Before the test, the damage is preliminarily identified as 7.7 m away from the top of the pile by the ultrasonic emission method (Mutlib *et al*. 2016, Shah and Ribakov 2010), which is also taken as the theoretical result for comparison. The response of the stress wave is excited by a hammer and measured by an ICP accelerometer with a sensitivity of 19.1 mV/m/s^2, which is installed on the pile head and shown in Fig. 25. The wave propagation velocity c is set as 4300 m/s based on the properties of the reinforced concrete pile. The data acquisition system used here is the LPT-EA pile integrity tester manufactured by the Shanghai Ruixin Company in China. The acceleration response is measured with a time interval of 21 μs, that is, the sampling frequency is 48 kHz. By integrating the collected acceleration data, the velocity curve is obtained and plotted in Fig. 26.

The CCWT with complex Gaussian wavelet as parent wavelet function is performed on the velocity response signal in Fig. 26 and the resultant wavelet scalogram is plotted in Fig. 27. It can be seen from Fig. 27 that there are two bright energy concentrating areas in the time frequency plane. However, it is quite difficult to accurately choose the time coordinates from the two bright energy concentrating regions by direct visualization. Thus, the K-means clustering algorithm and FFT are used to address this issue. First, the wavelet scalogram is split into two parts vertically by a straight red line (t = 10 ms). The left and right parts represent the first and second energy concentrating areas caused by the incident wave and reflected wave, respectively. Second, the critical threshold of the modulus of wavelet coefficients in the first energy concentrating region is set to be 0.00006, while that of the second concentrating region is defined as 0.000015. On a basis of this, the wavelet coefficient modulus larger than the preset threshold, is highlighted and the corresponding points are clustered by the K-means clustering algorithm, with the results presented in Fig. 28. As shown in Fig. 28, the time coordinates of the two clustering centers are 5.29 ms and 16.17 ms, respectively. To be specific, the clustering center at 5.29 ms is caused by the incident wave, while the clustering center at 16.17 ms is induced by the reflected wave at the bottom of the pile. The velocity response signal shown in Fig. 26 is also processed by FFT, leading to a Fourier spectrum as shown in Fig. 29. With a precise positioning of the first and last peak points in the Fourier spectrum, the frequency band of interest can be determined as 50 Hz~1600 Hz. Thus, the searching range of the crossing points is restricted to an area of 5.29 ms~16.17 ms and 50 Hz~1600 Hz in the time-frequency plane, which is called ABCD and shown in Fig. 30.

The phase angle is calculated according to Eq. (12) and the resultant instantaneous phase angles are mapped into the time-frequency plane and displayed in Fig. 30 in the manner of gray level. The crossing points are searched with a restriction of ABCD and two crossing points (Points 1 and

Fig. 25 The setup of the pile test

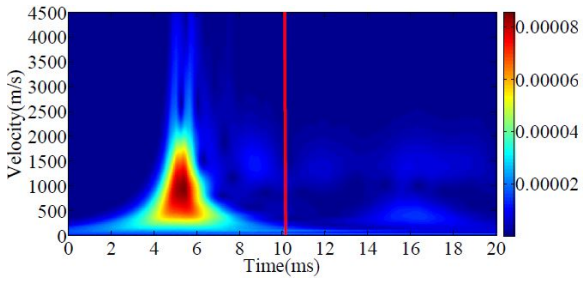

Fig. 27 The wavelet scalogram of the velocity response signal

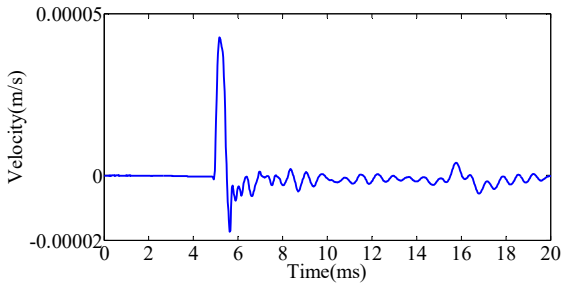

Fig. 26 The velocity response signal

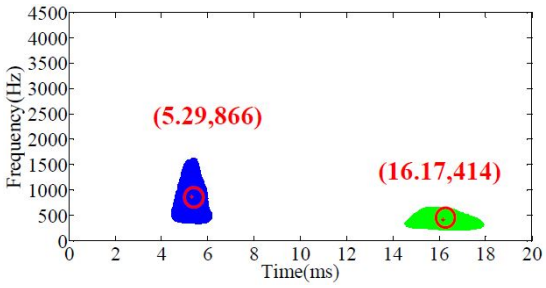

Fig. 28 The results after the K-means clustering

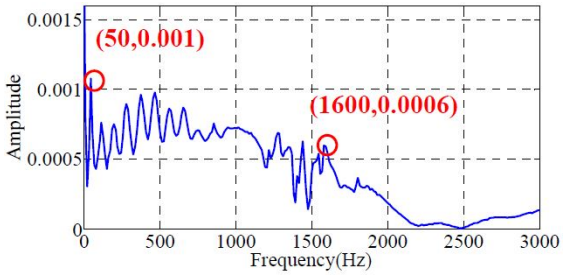

Fig. 29 The Fourier spectrum

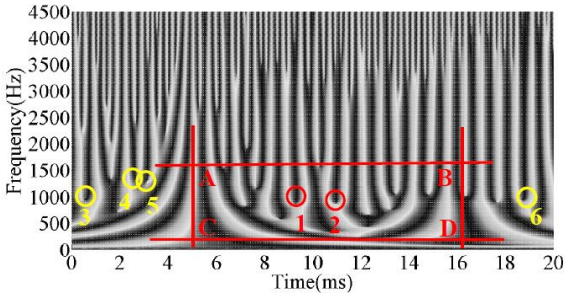

Fig. 30 The grayscale images of phase angles

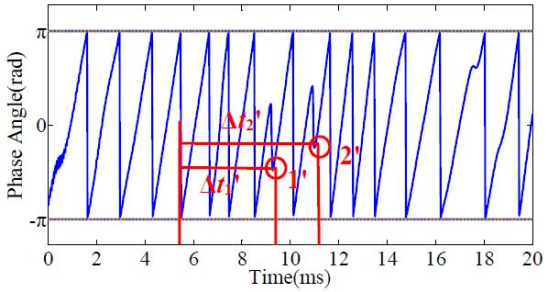

Fig. 31 The time-phase angle curve at the frequency of 865 Hz

2), whose frequency coordinates both correspond to around 828 Hz~865 Hz, are obtained. To further verify these two crossing points, the time-phase angle curve at a specific frequency of 865 Hz is calculated and displayed in Fig 31. It can be seen from Fig. 31 that the phase angle turning point corresponding to Point 1 and 2 are Point 1' and 2', with their time coordinates are 9.5 ms and 11 ms, respectively. Therefore, the time duration between Point 1' and the first clustering center induced by the incident wave, denoted as $\Delta t_1'$, is 4.21 ms (9.5 – 5.29 = 4.21 ms). Similarly, the time duration between Point 2' and the first clustering center, denoted as $\Delta t_2'$, is 5.71 ms (11 – 5.29 = 5.71 ms). Due to that the wave propagation velocity c is 4300 m/s by using the properties of the reinforced concrete pile, L_1' equals 9.05 m by substituting $\Delta t_1'$ and c into Eq. (15). L_2' can be solved in a similar way and equals 12.27 m. Compared with the damage localization results using the ultrasonic emission method, Point 1' (9.05 m) not Point 2' (12.27 m) is closer to the theoretical damage position (7.7 m), which confirms Point 1' is the real phase angle turning point. The relative error between the results from the proposed method and the ultrasonic emission method is 17.53%. By contrast, the phase turning point 2' can be treated as an interference point, and the reduction of interference points needs to be realized by mutual verification with other pile damage localization methods, e.g., the ultrasonic wave method.

In addition to Points 1 and 2, there are other four crossing points, named as Point 3~6 in the grayscale image (Fig. 30). Fortunately, they all fall outside the range of ABCD and do not need a further verification. Therefore, the conclusion is demonstrated once again that the objective definition of the specific area (ABCD) enhances the accuracy of pile damage localization by reducing the number of crossing points.

5. Conclusions

An improved method for pile damage localization based on CCWT is proposed in this paper. The effectiveness and accuracy of the proposed method are verified by numerical examples and two actual piles and conclusions are drawn as follows.

(1) Compared with the CCWT, the proposed method introduces the K-means clustering algorithm and FFT. The K-means clustering algorithm is used to accurately calculate the time coordinates of the energy concentrating points caused by the incident and reflected waves, respectively. Thus, the subjectivity of selecting energy concentrating points by visual inspection is avoided. Meanwhile, FFT is employed to calculate the frequency spectrum of the response signal, by which the frequency band of interest is determined. Therefore, the influence of interference points can be reduced even eliminated by finding the phase turning points within the obtained time and frequency range.

(2) A parameter analysis is conducted to investigate how the damage depth and damage degree in piles affect the accuracy and effectiveness of the proposed method. The results demonstrate that the proposed method is able to localize the pile with a damage at least 2.5 m away from the pile head (0.5 m away from the soil surface) when the damage degree is as less as 5%.

(3) Dynamic tests of an actual square reinforced concrete pile and an actual circular reinforced concrete pile are employed to verify the effectiveness of the proposed method. Although the proposed method is capable of localizing actual piles more accurately than the CCWT method, there are still some interference points in the grayscale images of phase angles. If the proposed method is planned to be applied on practical engineering, the reduction and elimination of the interference points need to be addressed by mutual verification with other pile damage localization methods, e.g., the ultrasonic emission method.

Acknowledgments

This study is sponsored by the National Natural Science Foundation of China (NSFC) under Grants No. 51608122, China Postdoctoral Science Foundation under Grants No. 2018M632561 and the Outstanding Youth Fund of Fujian Agriculture and Forestry University under Grants No. XJQ201728.

References

Beheshti-Aval, S.B., Taherinasab, M. and Noori, M. (2011), "Using harmonic class loading for damage identification of plates by wavelet transformation approach", *Smart. Struct. Syst., Int. J.*, **8**(3), 46-50. https://doi.org/10.12989/sss.2011.8.3.253

Beskhyroun, S., Oshima, T. and Mikami, S. (2010), "Wavelet-based technique for structural damage detection", *Struct. Control. Hlth.*, **17**(5), 473-494. https://doi.org/10.1002/stc.316

Billet, P. and Sieffert, J.G. (1989), "Soil-sheet pile interaction in vibro-piling", *J. Geotech. Eng.*, **115**(8), 1085-1101. https://doi.org/10.1061/(ASCE)0733-9410(1989)115:8(1085)

Boulahbal, D., Golnaraghi M.F. and Ismail, F. (1999), "Amplitude and phase wavelet maps for the detection of cracks in geared systems", *Mech. Syst. Signal Pr.*, **13**(3), 423-436. https://doi.org/10.1006/mssp.1998.1206

Cabella, E. and Passalacqua, R. (1998), "Axially loaded pile numerical models vs. experimental data, Application of Numerical Methods to Geotechnical Problems", *Polytech. Univ. Milano*, *Udine*, pp. 97-106. https://doi.org/10.1007/978-3-7091-2512-0_9

Fomchenko, A.L., Belova, A.S., Bekhtereva, E.S. and Kwabia, T.F. (2018), "Analysis of the Fourier spectrum of the ν_2 inversion band of the $^{15}NHD_2$ molecule", *Russ. Phys. J.*, **61**(2), 287-291. https://doi.org/10.1007/s11182-018-1399-1

Kachanov, V.K., Sokolov, I.V., Fedorenko, S.A. and Lebedev, S.V. (2017), "Use of the impact-echo method for analyzing the integrity of driven reinforced concrete piles", *Measure. Techniq.*, **60**(4), 1-6. https://doi.org/10.1007/s11018-017-1207-2

Kanungo, T., Mount, D.M., Netanyahu, N.S., Piatko, C.D., Silverman, R. and Wu, A.Y. (2002), "An efficient K-means clustering algorithm: analysis and implementation", *IEEE. T. Pattern. Anal.*, **24**(7), 205-215. https://doi.org/10.1109/TPAMI.2002.1017616

Kim, D., Lee, J., Nsabimana, E. and Jung, Y.H. (2012), "Numerical analysis of suction pile behavior with different loading locations and displacement inclinations", *Ocean Syst. Eng., Int. J.*, **2**(3), 205-215. https://doi.org/10.12989/ose.2012.2.3.205

Liu, J., Guo, Z., Zhu, N., Zhao, H., Garg, A., Xu, L., Liu, T. and Fu, C. (2019a), "Dynamic response of offshore open-ended pile under lateral cyclic loadings", *J. Marine Sci. Eng.*, **7**(5), 1-19. https://doi.org/10.3390/jmse7050128

Liu, J.L., Wang, S.F., Zheng, J.Y., Chang, C.M., Wei, X.J. and Ren, W.X. (2019b), "Time-frequency signal processing for integrity assessment and damage localization of concrete piles", *Int. J. Struct. Stabil. Dyn.*, **20**(3), 1-24. https://doi.org/10.1142/S0219455420500200

Massoudi, N. and Teffera, W. (2014), "Non-destructive testing of piles using the low strain integrity method", *Proceedings of 5th International Conference on Case Histories in Geotechnical Engineering*, *Missouri University of Science and Technology*, Rolla, MO, USA, pp. 13-17.

Messina, A. (2008), "Refinements of damage detection methods based on wavelet analysis of dynamical shapes", *Int. J. Solids Struct.*, **45**(14), 4068-4097. https://doi.org/10.1016/j.ijsolstr.2008.02.015

Mutlib, N.K., Baharom, S.B., El-Shafie, A. and Nuawi, M.Z. (2016), "Ultrasonic health monitoring in structural engineering: buildings and bridges", *Struct. Control. Health Monit.*, **23**(3), 409-422. https://doi.org/10.1002/stc.1800

Nagayama, T., Sim, S.H., Miyamori, Y. and Spencer Jr, B.F. (2007), "Issues in structural health monitoring employing smart sensors", *Smart. Struct. Syst., Int. J.*, **3**(3), 299-320. https://doi.org/10.12989/sss.2007.3.3.299

Ni, S.H., Isenhower, W.M. and Huang, Y.H. (2012), "Continuous wavelet transform technique for low strain integrity testing of deep drilled shafts", *J. Geoeng.*, **7**(3), 97-105.

Ni, S.H., Yanga, Y.Z. and Tsai, P.H. (2017), "Evaluation of pile defects using complex continuous wavelet transform analysis", *NDT&E Int.*, **87**, 50-59. https://doi.org/10.1016/j.ndteint.2017.01.007

Niederleithinger, E. and Taffe, A. (2006), "Early stage elastic wave velocity of concrete piles", *Cem. Concr. Compos.*, **28**(4), 317-320. https://doi.org/10.1016/j.cemconcomp.2006.02.013

Olson, L.D. and Wright, C.C. (1989), "Nondestructive testing of deep foundations with sonic methods", *Proceedings of Foundation Engineering Congress: Current Principles and Practice*, Reston, pp. 1173-1183.

Park, H.C. and Kim, D.S. (2006), "Non-destructive pile integrity test using HWAW method", *Key Eng. Mater.*, **321-323**, 363-366. https://doi.org/10.4028/www.scientific.net/KEM.321-323.363

Poskitt, T.J. (1991), "Energy losses in pile-driving due to soil rate effects and hammer", *Proc. Inst. Civ. Eng.*, **91**(4), 823-851. https://doi.org/10.1680/iicep.1991.17492

Rausche, F., Shen, R.K., Likins Jr, G.E. (1991), "Comparison of pulse echo and transient response pile integrity test methods", *Transp. Res. Rec.*, **1331**, 21-27.

Seyedpoor, S.M., Norouzi, E. and Ghasemi, S. (2018), "Structural damage detection using a multi-stage improved differential evolution algorithm (Numerical and experimental)", *Smart. Struct. Syst., Int. J.*, **21**(2), 235-248. https://doi.org/10.12989/sss.2018.21.2.235

Shah, A.A. and Ribakov, Y. (2010), "Effectiveness of nonlinear ultrasonic and acoustic emission evaluation of concrete with distributed damages", *Mater. Des.*, **31**(8), 3777-3784. https://doi.org/10.1016/j.matdes.2010.03.020

Take, W.A., Valsangkar, A.J. and Randolph, M.F. (1999), "Analytical solution for pile hammer impact", *Comput. Geotech.*, **25**(2), 57-74. https://doi.org/10.1016/S0266-352X(99)00018-X

Wolf, J.P and Arx, G.A.V. (1982), "Travelling waves in a group of piles taking pile-soil-pile interaction into account", *Earthq. Eng. Struct. Dyn.*, **10**(2), 225-237.

Xu, J., Ren, Q. and Shen, Z. (2016), "Low strain pile testing based on synchrosqueezing wavelet transformation analysis", *J. Vibroeng.*, **18**(2), 813-825.

Zhang, Y., Fan, Y., Li, Z., Wang, C. and Ding, X. (2020), "Wave propagation in X-section piles for low strain integrity testing: three-dimensional effects", *Shock Vib.* https://doi.org/10.1155/2020/7574654

Zheng, W., Wang, S., Lin, C., Yu, X. and Liu, J. (2020), "Damage localization of piles based on complex continuous wavelet transform: numerical example and experimental verification", *Shock Vib.* https://doi.org/10.1155/2020/8058640

HJ